AIP Journal of Applied Physics

Phase field simulations of ferroelectric nanoparticles with different long-range-electrostatic and -elastic interactions

Jie Wang, Marc Kamlah, and Tong-Yi Zhang

Citation: Journal of Applied Physics **105**, 014104 (2009); doi: 10.1063/1.3043576
View online: http://dx.doi.org/10.1063/1.3043576
View Table of Contents: http://scitation.aip.org/content/aip/journal/jap/105/1?ver=pdfcov
Published by the AIP Publishing

Phase field simulations of ferroelectric nanoparticles with different long-range-electrostatic and -elastic interactions

Jie Wang,[1,2,a] Marc Kamlah,[2] and Tong-Yi Zhang[1]
[1]*Department of Mechanical Engineering, Hong Kong University of Science and Technology, Clear Water Bay, Kowloon, Hong Kong, China*
[2]*Institute for Materials Research II, Forschungszentrum Karlsruhe, Postfach 3640, 76021 Karlsruhe, Germany*

(Received 12 June 2008; accepted 3 November 2008; published online 12 January 2009)

Two-dimensional phase field simulations of ferroelectric nanoparticles with different long-range (LR)-electrostatic and -elastic interactions and different domain wall energy densities are conducted based on the time-dependent Ginzburg–Landau equation. The phase field simulations exhibit vortex patterns of polarizations, which have purely toroidal moments of polarizations and macroscopically negligible averaged polarizations, in nanoparticles without or with weak LR-elastic interactions when LR-electrostatic interactions are fully taken into account. However, a single-domain structure without any toroidal moment of polarizations is formed in small nanoparticles if LR-electrostatic interactions are completely ignored or LR-elastic interactions are fully taken into account. The polarization gradient energy or domain wall energy density plays also an important role in the formation of polarization structure. The vortex structure transits from a multivortex structure to a single-vortex structure as the domain wall energy density increases. © *2009 American Institute of Physics*. [DOI: 10.1063/1.3043576]

I. INTRODUCTION

Ferroelectric properties in low-dimensional structures, such as ferroelectric epitaxial islands[1–4] and thin films,[5–8] ferroelectric nanotubes and nanorods,[9,10] and ferroelectric particles,[11,12] have been investigated with a great deal of interest due to the potential integration of nanoscale ferroelectrics into micro/nanoelectronics. Both long-range (LR)-electrostatic and -elastic interactions play critical roles in the formation of polarization patterns in low-dimensional ferroelectric structures. LR-electrostatic interactions make the 180° stripe domains energetically favorable in ferroelectric thin films[7] and make it possible to quench spontaneous polarization.[13,14] LR-elastic interactions make the 90° domains energetically favorable in mechanically constrained ferroelectrics.[15] Polarization patterns in a ferroelectric particle could be complex,[16] which results from the competition among LR-elastic and -electrostatic interactions, domain wall energy, and other kinds of energies.

Although electrical and mechanical off-center structural distortions in a ferroelectric lattice cell are characterized by spontaneous polarization (electric dipole) and spontaneous strains, respectively, spontaneous strains are determined by spontaneous polarization. Spontaneous strains at stress-free state are called eigenstrains, which may lead to LR-elastic interactions in a ferroelectric nanoparticle of multiple lattice cells. If there is an inhomogeneous spontaneous strain field in a freestanding ferroelectric nanoparticle, an internal stress field may be generated even though the nanoparticle is freestanding without any external mechanical loads and traction-free without any mechanical constraints. The traction-free condition does not guarantee the ferroelectric nanoparticle to be stress-free because the stress field generated by an inhomogeneous spontaneous strain field is internal, which is self-balanced. Rather, the traction-free condition makes an internal stress field weaker in comparison with that under mechanical constraints. Clearly, an internal stress field in a ferroelectric nanoparticle depends on the particle size, the magnitude of spontaneous strains, the elastic constants of the particle, and the distribution of polarizations in the particle, which depends on the LR-electrostatic interactions of polarizations. The electrical boundary condition plays an important role in the LR-electrostatic interactions of polarizations. The ideal open-circuit electric boundary condition leads to a depolarization field and the strongest LR-electrostatic interactions, while the ideal short-circuit electric boundary condition nulls the depolarization field and weakens the LR-electrostatic interactions. Ponomareva *et al.*[17] studied the effect of different electrical and mechanical boundary conditions on low-dimensional ferroelectrics via Monte Carlo simulations by using a first-principles-based effective Hamiltonian, in which all strain components are allowed to relax completely for a freestanding system. As mentioned above, an internal stress field may exist in a freestanding ferroelectric nanoparticle. The present work aims to investigate, by using phase field simulations, the roles of LR-elastic and -electrostatic interactions in the formation of polarization patterns in ferroelectric nanoparticles under different electrical boundary conditions.

The phase field model used here is the same as that developed in our previous work,[14] which is based on the time-dependent Ginzburg–Landau equation. Compared to other phase field methods,[18–22] we do not impose periodic boundary conditions to the simulated system and solve LR-elastic and -electrostatic interactions in real space rather than

[a]Author to whom correspondence should be addressed. Tel.: +49-7247-82-5857. FAX: +49-7247-82-2347. Electronic mail: jie.wang@imf.fzk.de.

in reciprocal space. In real space, one can apply any type of electrical and mechanical boundary conditions on the surfaces of a finite-size ferroelectric. In the present work, the traction-free boundary condition is applied to the ferroelectric nanoparticles, thereby indicating that the nanoparticle is freestanding. Since in-real-space calculations of LR-elastic and -electrostatic interactions are very time-consuming, we conduct two-dimensional (2D) simulations with plane strains condition here to demonstrate the formation mechanism of polarization patterns and the role of LR-elastic and -electrostatic interactions.

In the present work, we study the effects of LR-elastic and -electrostatic interactions on the formation of polarization patterns by varying the strengths of LR-elastic and -electrostatic interactions with weight parameters α and β, respectively, which are correspondingly assigned to the electrostrictive coefficients and the electrostatic energy. Six cases are studied here with (i) $\alpha=0$ and $\beta=0$, (ii) $\alpha=0$ and $\beta=1$, (iii) $\alpha=1$ and $\beta=0$, (iv) $\alpha=1$ and $\beta=1$, (v) $\alpha=0.5$ and $\beta=0$, and (vi) $\alpha=0.5$ and $\beta=1$. The weight parameter $\alpha=0$ represents the stress-free condition, in which there are no LR-elastic interactions at all, while $\alpha=1$ represents that a ferroelectric nanoparticle has the values of electrostrictive coefficients, which are currently used in phase field simulations in literature.[15,18] We vary parameter α from 0 to 1 in the simulations and $\alpha=1$ corresponds that LR-elastic interactions are fully taken into account. In this sense, $\alpha=0.5$ represents that a ferroelectric nanoparticle has half values of the currently used electrostrictive coefficients or only a half of LR-elastic interactions is taken into account. Similarly, the weight parameter $\beta=1$ represents the ideal open-circuit electrical boundary condition, in which LR-electrostatic interactions are fully taken into account without any screening of depolarization field. On contrast, $\beta=0$ corresponds to the ideal short-circuit electrical boundary condition, in which LR-electrostatic interactions disappear completely. It should be noted that the LR-elastic and -electrostatic interactions in freestanding nanoparticles are attributed to spatially inhomogeneous spontaneous strains and polarization-induced charges, respectively. For order-disorder ferroelectrics, there is no spontaneous strain and thus the LR-elastic interaction disappears. This corresponds to the case of $\alpha=0$ in the present study. On the other hand, ferroelectrics sometimes are not ideal insulator. The polarization-induced charges inside the material can be compensated by external free charges under the short-circuited electrical boundary condition. So there is no internal electric field and the LR-electrostatic interaction disappears, which corresponds to the case of $\beta=0$ in the present study.

II. SIMULATION METHODOLOGY

In ferroelectric phase-field simulations,[14–16,18–22] it is usually assumed that equilibrium states in mechanical and electrical fields are established instantaneously for a given distribution of spontaneous polarizations at each time step of polarization evolution. Thus, spontaneous polarization $\mathbf{P}=(P_1,P_2,P_3)$ is the only order parameter and the temporal evolution of spontaneous polarizations is calculated from the time-dependent Ginzburg–Landau equation,

$$\frac{\partial P_i(\mathbf{r},t)}{\partial t} = -L\frac{\delta F}{\delta P_i(\mathbf{r},t)} \quad (i=1,2,3), \tag{1}$$

where L is the kinetic coefficient, $\mathbf{r}=(x_1,x_2,x_3)$ denotes the spatial vector, t is time, and F is the total fee energy. The total free energy in a simulated ferroelectric nanoparticle can be expressed as

$$F = \int_V [f_{\mathrm{Lan}}(P_i) + f_{\mathrm{Ela}}(\sigma_{ij}) + f_{\mathrm{Cou}}(\sigma_{ij},P_i) + f_{\mathrm{Gra}}(P_{i,j}) + \beta f_{\mathrm{Dep}}(E_i^d,P_i)]dV, \tag{2}$$

in which f_{Lan}, f_{Ela}, and f_{Cou} are the Landau free energy density, elastic energy density, and coupling energy density, respectively, which can be expressed by[23]

$$f_{\mathrm{Lan}}(P_i) = \alpha_1(P_1^2+P_2^2+P_3^2) + \alpha_{11}(P_1^4+P_2^4+P_3^4) + \alpha_{12}(P_1^2P_2^2+P_2^2P_3^2+P_1^2P_3^2) + \alpha_{111}(P_1^6+P_2^6+P_3^6) + \alpha_{112}[(P_1^4\ (P_2^2+P_3^2) + P_2^4(P_1^2+P_3^2) + P_3^4(P_1^2+P_2^2)] + \alpha_{123}P_1^2P_2^2P_3^2, \tag{3}$$

$$f_{\mathrm{Ela}}(P_i,\sigma_{ij}) = -\tfrac{1}{2}s_{11}(\sigma_{11}^2+\sigma_{22}^2+\sigma_{33}^2) - s_{12}(\sigma_{11}\sigma_{22}+\sigma_{22}\sigma_{33}+\sigma_{11}\sigma_{33}) - \tfrac{1}{2}s_{44}(\sigma_{12}^2+\sigma_{23}^2+\sigma_{13}^2), \tag{4}$$

$$f_{\mathrm{Cou}}(P_i,\sigma_{ij}) = -Q_{11}(\sigma_{11}P_1^2+\sigma_{22}P_2^2+\sigma_{33}P_3^2) - Q_{12}[\sigma_{11}(P_2^2+P_3^2)+\sigma_{22}(P_1^2+P_3^2)+\sigma_{33}(P_1^2+P_2^2)] - Q_{44}(\sigma_{12}P_1P_2+\sigma_{13}P_1P_3+\sigma_{23}P_2P_3), \tag{5}$$

where $\alpha_1=(T-T_0)/2\varepsilon_0C_0$ is the dielectric stiffness, α_{11}, α_{12}, α_{111}, α_{112}, and α_{123} are the higher order dielectric stiffnesses, T and T_0 denote temperature and the Curie–Weiss temperature, respectively, C_0 is the Curie constant, Q_{ij} are the electrostrictive coefficients, s_{ij} are the elastic compliances, and σ_{ij} are stresses. The term of $f_G(P_{i,j})$ in Eq. (2) is the gradient energy density[15,16] with the form

$$f_G(P_{i,j}) = \tfrac{1}{2}G_{11}(P_{1,1}^2+P_{2,2}^2+P_{3,3}^2) + G_{12}(P_{1,1}P_{2,2}+P_{2,2}P_{3,3}+P_{1,1}P_{3,3}) + \tfrac{1}{2}G_{44}[(P_{1,2}+P_{2,1})^2+(P_{2,3}+P_{3,2})^2+(P_{1,3}+P_{3,1})^2] + \tfrac{1}{2}G'_{44}[(P_{1,2}-P_{2,1})^2+(P_{2,3}-P_{3,2})^2+(P_{1,3}-P_{3,1})^2], \tag{6}$$

where G_{11}, G_{12}, G_{44}, and G'_{44} are gradient energy coefficients, and $P_{i,j}$ denotes the derivative of the ith component of the polarization vector P_i with respect to the jth coordinate and i, $j=1$, 2, and 3. The last term f_{Dep} in Eq. (2) is the LR-electrostatic interaction energy density. Without any applied electric field, we have[24]

$$f_{\mathrm{Dep}} = -\tfrac{1}{2}(E_1^d P_1 + E_2^d P_2 + E_3^d P_3), \tag{7}$$

where E_1^d, E_2^d, and E_3^d are three components of a depolarization field along the x_1, x_2, and x_3 axes, respectively. The finite difference method for spatial derivatives and the Runge–Kutta method of order four for temporal derivatives are employed to solve Eq. (1) in real space with the boundary condition of $dP_i/dn=-P_i/\delta$, in which n refers to unit length in the normal direction of the surface and δ is the extrapolation length.

In the present study, the same method used in Ref. 14 is adopted to calculate electrostatic field and stress field with the exception that weights α and β are assigned to the electrostrictive coefficients Q_{ijkl} and the LR-electrostatic interaction energy density, respectively, to control correspondingly the strengths of LR-electrostatic and -elastic interactions. Internal stresses are calculated from $\sigma_{ij}=c_{ijkl}(\varepsilon_{kl}-\varepsilon_{kl}^0)$, in which c_{ijkl}, ε_{kl}, and ε_{kl}^0 denote the elastic constants, the total strains, and the spontaneous strains, respectively. The spontaneous strains relate to spontaneous polarizations as $\varepsilon_{ij}^0=\alpha Q_{ijkl}P_kP_l$. When weight parameter α varies from zero to one, electrostrictive coefficients αQ_{ijkl} change from zero to Q_{ijkl}. Mechanical stresses must satisfy the mechanical equilibrium equation of $\sigma_{ij,j}=0$, which is numerically solved by using the finite element method for a given polarization distribution with the traction-free boundary condition.

We divide polarizations into two parts: the spontaneous and induced polarizations. Since the spontaneous polarizations are embedded inside a paraelectric medium, the induced polarizations are linearly proportional to the electric field. Thus, the electrostatic equilibrium equation, $\mathbf{D}_{i,i}=(\varepsilon_0\kappa\mathbf{E}+\mathbf{P})_{i,i}=0$ must be satisfied for a body-charge-free paraelectric medium,[22–24] where $\varepsilon_0=8.85\times10^{-12}$ F m^{-1} is the dielectric constant of vacuum and κ denotes the relative dielectric constant tensor of the background material. In this way, the potential of a depolarization field can be calculated from

$$\varepsilon_0\kappa(\phi_{,11}+\phi_{,22}+\phi_{,33}) = P_{1,1}+P_{2,2}+P_{3,3} \tag{8}$$

for a given spontaneous polarization field, in which the depolarization field is defined as the negative gradient of an electrostatic potential ϕ, i.e., $E_i^d=-\phi_{,i}$. Since the background material is the paraelectric phase, which has a cubic crystal structure, the relative dielectric constant matrix is diagonal and the relative dielectric constants in three axis directions are the same, i.e., $\kappa=\kappa_{11}=\kappa_{22}=\kappa_{33}$ and $\kappa_{ij}=0(i\neq j)$. The electrostatic equilibrium equation (8) is solved by using the finite difference method for a given polarization distribution with the electrical open-circuit boundary condition.

Dimensionless variables[15] are used in the present simulations. The material constants adopted in the present simulations are the same as those used in Ref. 14 and the simulated nanoparticles are at room temperature. The value of the extrapolation length δ is taken to be 3 in the present study.[12] We use 20×20 discrete grids to represent a 2D square particle and each grid has a dimensionless area of $a\times a$. The grid size a is assigned different values to represent different sizes of ferroelectrics. The polarization varies spatially and is characterized at each grid by a two-component vector, or an electric dipole, of which the length and direction denote the magnitude and direction of the dipole, respectively. The dimensionless time step is set to be $\Delta t=0.004$ and the total number of steps in solving Eq. (1) is 8000, which is sufficient to allow the simulated system to reach a steady state.[15] In the following, we report simulation results at the steady state only.

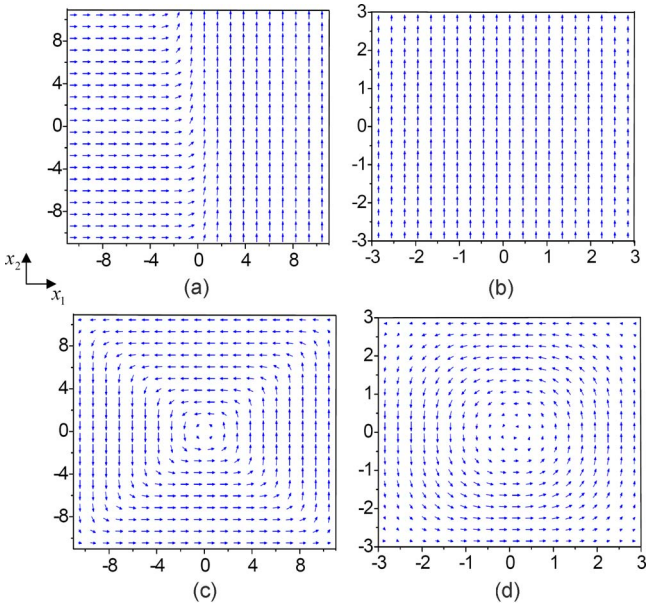

FIG. 1. (Color online) Size dependence of polarization patterns in stress-free ($\alpha=0$) 2D ferroelectric nanoparticles with $\beta=0$ in (a) and (b) and $\beta=1$ in (c) and (d).

III. SIMULATION RESULTS

A. Stress-free ferroelectric nanoparticles with $\alpha=0$

When the weight parameter $\alpha=0$, ferroelectric nanoparticles are stress-free and the stress related energies disappear, i.e., the elastic energy density and the coupling energy density become zero. Figures 1(a)–1(d) show the polarization patterns of the stress-free ($\alpha=0$) 2D square ferroelectrics with $\beta=0$ and 1, respectively, where Figs. 1(a) and 1(c) are for the simulated dimensionless size of 22 and Figs. 1(b) and 1(d) are for the size of 6, respectively, with one unit in the dimensionless size corresponding to 1 nm in the real size.[16] As mentioned above, the case of $\beta=0$ represents the ideal short-circuit electrical boundary condition, in which there is no electrostatic interaction. In the nanoparticle with a dimensionless size of 22, the polarizations form two domains with a 90° domain wall, which is almost perpendicular to the polarizations in one domain and parallel to the polarizations in the other domain. This kind of a 90° domain wall is different from the normal 90° domain wall induced by LR-elastic interactions, in which the wall has an angle of 45° with polarizations in both domains. When LR-electrostatic interactions are taken into account, the normal components of polarizations should be continuous. The polarization structure shown in Fig. 1(a) is formed due to the lack of LR-electrostatic interactions and the reduction in the Landau free energy. With the size decreasing, the gradient energy becomes predominate in comparison with the Landau free en-

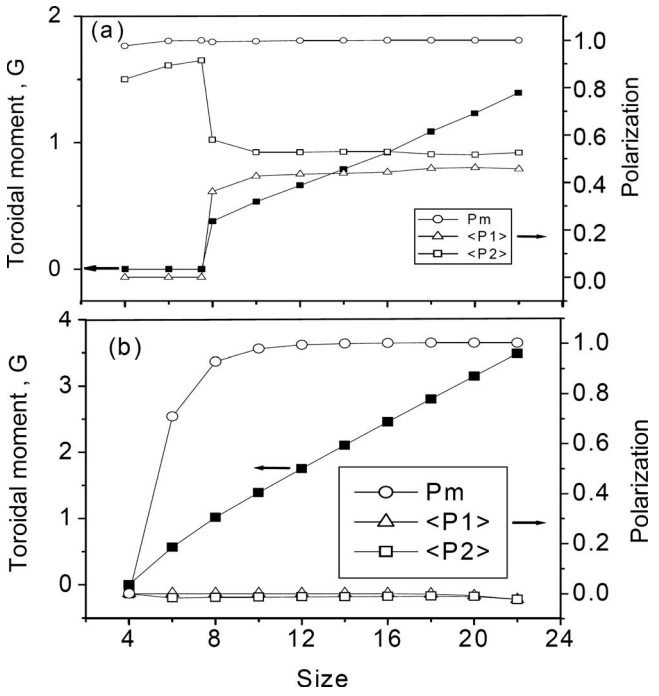

FIG. 2. The polarization moment G on the left vertical axis, and the macroscopically averaged polarization components, $\langle P_1 \rangle$ and $\langle P_2 \rangle$, and the magnitude of the maximum polarization P_m on the right vertical axis as functions of the sizes of the simulated stress-free ($\alpha=0$) ferroelectric nanoparticles with $\beta=0$ in (a) and $\beta=1$ in (b)

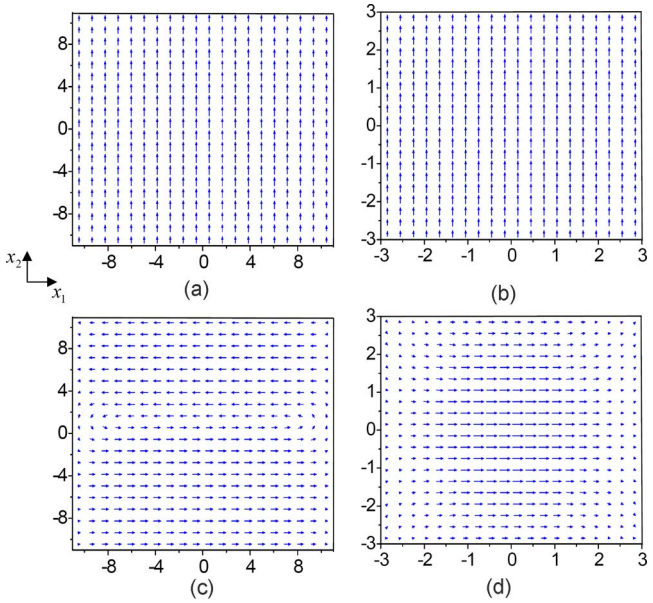

FIG. 3. (Color online) Size dependence of polarization patterns in 2D ferroelectric nanoparticles with $\beta=0$ in (a) and (b) and $\beta=1$ in (c) and (d) when LR-elastic interactions are fully taken into account ($\alpha=1$).

ergy, therefore, the polarization pattern changes from the multidomain state to the monodomain state. Figure 1(b) shows the monodomain structure with a dimensionless particle size of 6. No vortex structure exhibits in Figs. 1(a) and 1(b) due to the absence of LR-electrostatic interactions for both sizes. The case of $\beta=1$ corresponds to the ideal open-circuit electrical boundary condition, in which LR-electrostatic interactions are fully taken into account. Under the ideal open-circuit electrical boundary condition, polarizations form a vortex pattern, as shown in Figs. 1(c) and 1(d), and the macroscopically averaged polarization, defined as $\langle \mathbf{p} \rangle = (N)^{-1} \Sigma_k \mathbf{p}_k$,[25] is found to be zero, i.e., $\langle \mathbf{P} \rangle = 0$. The vortex pattern may also be regarded as having a domain structure with four domains and four wide 90° domain walls, which is caused by the square shape of the simulated ferroelectrics. The width of the domain walls highly depends on the polarization gradient energy density[15,16] and on the simulated ferroelectric size. When the particle size is reduced from 22 to 6, the 90° domain structure becomes obscure and the vortex pattern is more distinct.

Figures 2(a) and 2(b) illustrate the toroidal moment of polarizations G, the macroscopically averaged polarization components $\langle P_1 \rangle$ and $\langle P_2 \rangle$, and the magnitude of the maximum polarization $p_m = \max\{|\mathbf{p}_k|\}$ in stress-free ($\alpha=0$) ferroelectric particles as a function of the particle size for $\beta=0$ and 1, respectively. The toroidal moment of polarizations $\mathbf{G}$ is defined as $\mathbf{G} = (2N)^{-1} \Sigma_i \mathbf{R}_i \times \mathbf{p}_i$, where $\mathbf{p}_i$ is the local dipole of cell i located at $\mathbf{R}_i$, and N is the number of cells in the simulations. In the case of $\beta=0$, the polarization pattern changes from the multidomain state to the monodomain state as the size is reduced to 8, which results in the abrupt disappearance of the toroidal moment of polarizations, as shown in Fig. 2(a). The maximum polarization P_m and the macroscopically averaged polarization component $\langle P_2 \rangle$ are both nonzero, as shown in Fig. 2(a). Furthermore, the magnitude of the maximum polarization still has a high value even at the size of 4, at which the macroscopically averaged polarization components are both zero in the case of $\beta=1$, as shown in Fig. 2(b). When $\beta=1$, both the moment and the magnitude of the maximum polarization decrease with the decrease in the particle size and become zero at the size of 4, as shown in Fig. 2(b). With $\beta=1$, the polarizations form a vortex for all simulated sizes and the macroscopically averaged polarization components, $\langle P_1 \rangle$ and $\langle P_2 \rangle$, are almost equal to zero, thereby indicating that the vortex pattern does not exhibit any macroscopically averaged polarizations. The vortex pattern without any macroscopically averaged polarizations is very important for memory nanodevices.[25] The polarizations without any macroscopically averaged polarization components do not produce a strong electric field that has a LR character. The vortex structure with a purely toroidal moment of polarizations in a nanoparticle can therefore be switched without disturbing the states of its neighboring particles. Consequently, the nanoparticles as toroidal moment carriers can thus be packed more densely than the conventional carriers of macroscopic polarizations, which will make a remarkable improvement in the density of ferroelectric recording.

B. Ferroelectric nanoparticles with $\alpha=1$

When $\alpha=1$, the currently used values of electrostrictive coefficients are employed in the simulations, in which the spontaneous strain is the largest among the three α's. In this case, even in a freestanding and traction-free nanoparticle, an internal stress field is generated if the polarization distribution is inhomogeneous. Figures 3(a)–3(d) show polarization

patterns in the 2D square ferroelectrics with $\alpha=1$ for $\beta=0$ and 1, respectively, where Figs. 3(a) and 3(c) are for the simulated dimensionless size of 22 and Figs. 3(b) and 3(d) are for the size of 6, respectively. When $\beta=0$, there are no LR-electrostatic interactions in the simulated ferroelectrics, the polarizations form a monodomain pattern, as shown in Figs. 3(a) and 3(b), and the toroidal moment of polarization is found to be zero, i.e., $\mathbf{G}=0$. A monodomain pattern has a much lower elastic energy than a multidomain pattern because the spontaneous polarizations in a monodomain ferroelectric particle are almost homogeneous except for slight variations in magnitude of polarizations at the four boundaries of the particle. A homogeneous spontaneous polarization field induces a homogeneous spontaneous strain field in a freestanding nanoparticle, which makes it stress-free without any internal stresses. When the size of simulated ferroelectric nanoparticles is reduced from 22 to 6, the polarization pattern remains in a monodomain structure but the magnitude of polarizations becomes smaller. When $\beta=1$, LR-electrostatic interactions are fully taken into account and the ferroelectric particle with the size of 6 still has a monodomain pattern, as shown in Fig. 3(d). However, a two-domain structure with a 180° domain wall is formed for the nanoparticle with the size of 22, in which one domain is parallel to the x_1-axis and the other is antiparallel to the x_1-axis, as shown in Fig. 3(c). The appearance of the 180° domain wall is attributed to the reduction in the LR-electrostatic interaction energy, which is induced by the depolarization field. The elastic energy will be reduced when the size of a freestanding nanoparticle is small. That is why a monodomain structure is formed when the size is 6, as shown in Fig. 3(d). Any inhomogeneity in the direction and magnitude of spontaneous polarizations generates an internal stress field if there are spontaneous strains associated with the polarizations. Any inhomogeneity in the direction and magnitude of spontaneous polarizations may also generate a depolarization field and thus induces LR-electrostatic interactions if the induced charges are not fully screened. The tail-to-head polarization pattern and the vortex structure are predominately determined by LR-electrostatic interactions.

Figures 4(a) and 4(b) show the size dependences of the toroidal moment of polarization, the macroscopically averaged polarizations, and the magnitude of the maximum polarization with the β values of 0 and 1, respectively. When $\beta=0$, the macroscopically averaged polarization $\langle P_2\rangle$ decreases if the size decreases, as shown in Fig. 4(a). Without LR-electrostatic interactions, the polarizations in every simulated nanoparticle form a single domain pattern within the size range from 4 to 22 and the toroidal moment of polarizations is zero. This fact indicates that LR-electrostatic interactions are necessary to form a vortex pattern in ferroelectric particles. This conclusion is further verified in the case of $\beta=1$. With LR-electrostatic interactions of $\beta=1$, the polarization pattern changes from the multidomain state to the monodomain state as the size is reduced from 22 to 12, which results in the abrupt disappearance of the toroidal moment of polarizations, as shown in Fig. 4(b). Further decreasing the size reduces the magnitude of the maximum spontaneous polarization P_m and may eventually change the

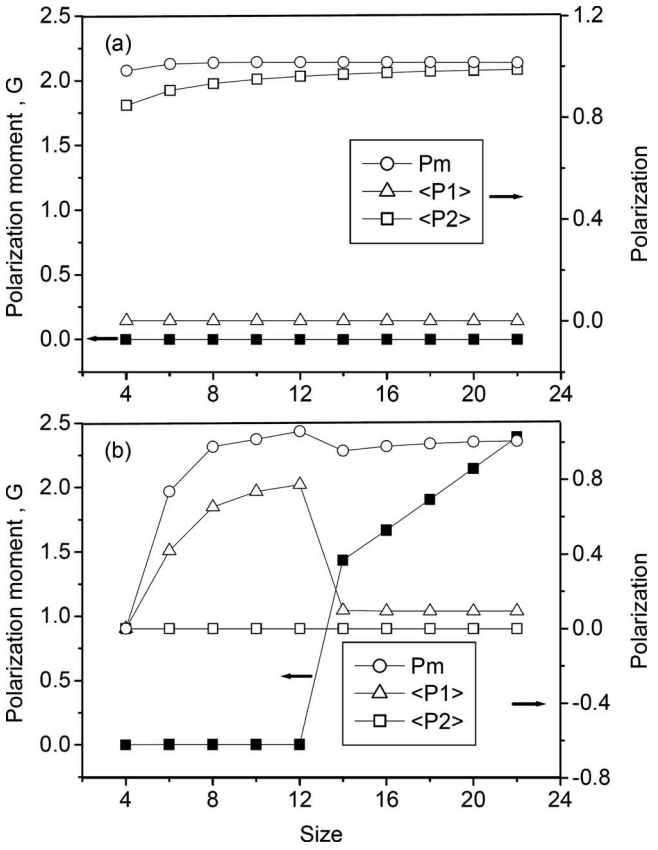

FIG. 4. The polarization moment G on the left vertical axis, and the macroscopically averaged polarization components, $\langle P_1\rangle$ and $\langle P_2\rangle$, and the magnitude of the maximum polarization P_m on the right vertical axis as functions of the sizes of the simulated ferroelectric nanoparticles with $\beta=0$ in (a) and $\beta=1$ in (b) when LR-elastic interactions are fully taken into account ($\alpha=1$).

simulated system from the ferroelectric phase with a monodomain state to the paraelectric phase at the size of 4. The critical size for the ferroelectric/parallectric phase transition is highly dependent on the value of the extrapolation length, which is not discussed in the present study.

C. Ferroelectric nanoparticles with $\alpha=0.5$

When $\alpha=0.5$, a half of the currently used values of electrostrictive coefficients is employed in the simulations. Figures 5(a) and 5(b) show the size dependence of polarization patterns in the simulated nanoparticles with $\alpha=0.5$ under the short-circuit boundary condition. For the case of $\alpha=0.5$, there exists an internal stress field in a freestanding ferroelectric nanoparticle, but the strength of internal stress field is lower than that in the case of $\alpha=1$. However, a two-domain structure with a 90° domain wall is still formed in a nanoparticle with the size of 22, as shown in Fig. 5(a). Due to the lack of LR-electrostatic interactions, the polarizations from the two domains seem to merge into the domain wall, as illustrated in Fig. 5(a), which is different from the head-to-tail arrangements in the domain walls shown in Figs. 1(c) and 3(c). When the nanoparticle size decreases to 6, the polarizations form a single-domain structure, as shown in Fig. 5(b). Figures 1(b), 3(b), and 5(b) show a similar single-domain structure in the nanoparticles having the same size of

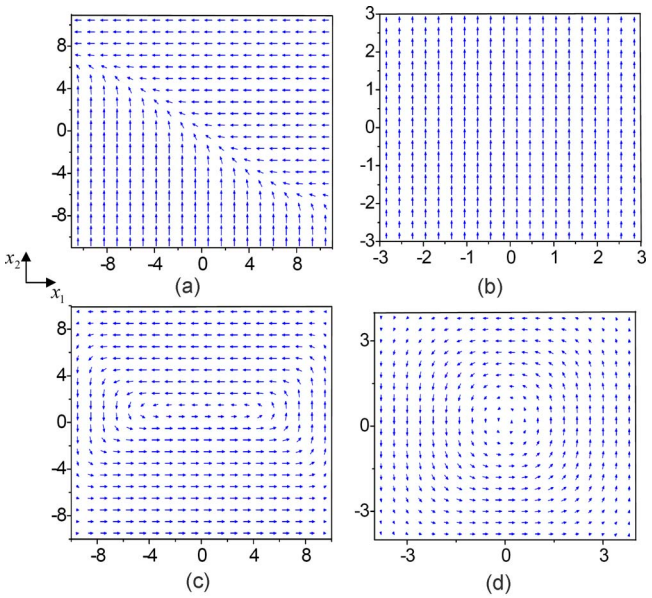

FIG. 5. (Color online) Size dependence of polarization patterns in 2D ferroelectric nanoparticles with $\beta=0$ in (a) and (b) and $\beta=1$ in (c) and (d) when a half level of LR-elastic interactions is taken into account ($\alpha=0.5$).

6 but with different levels of elastic interactions under the short-circuit boundary condition. This fact indicates that the role of LR-elastic interactions is not crucial in the formation of polarization patterns in small freestanding ferroelectric nanoparticles without LR-electrostatic interactions. Figures 5(c) and 5(d) illustrate the polarization patterns with $\alpha=0.5$ under the open-circuit boundary condition for the simulated sizes of 20 and 8, respectively. Comparing Fig. 5(d) with Fig. 1(d) indicates that the vortex pattern for the small size with $\alpha=0.5$ is almost the same as that for $\alpha=0$. However, Fig. 5(c) shows different vortex patterns from that shown in Fig. 1(c). In Fig. 5(c), the two domains parallel and antiparallel to the x_2-axis shrink and the two domains parallel and antiparallel to the x_1-axis grow such that there forms a 180° domain wall between them. When the spontaneous strains become higher, two domains parallel and antiparallel to the x_1-axis grow further, and eventually, the two domains parallel and antiparallel to the x_2-axis disappear, as shown in Fig. 3(c) for $\alpha=1$, where a 180° domain structure exists. The change in the polarization pattern is caused by the elastic energy induced by LR-elastic interactions.

Figures 6(a) and 6(b) give the size-dependent behaviors of the toroidal moment, the macroscopically averaged polarization, and the magnitude of the maximum polarization in the case of $\alpha=0.5$ under the short-circuit condition and the open-circuit condition, respectively. Figure 6(a) shows the drop down in the toroidal moment and the two macroscopically averaged polarization components when the size decreases from 22 to 20, which corresponds to the change in the domain structure from the multidomain state to the monodomain state. The size dependence of the toroidal moment and the magnitudes of the maximum polarization in Fig. 6(b) are similar to those in Fig. 2(b) for the case of $\alpha=0$. For a given simulated size, however, the magnitude of the toroidal moment for the case of $\alpha=0.5$ is smaller than that for the

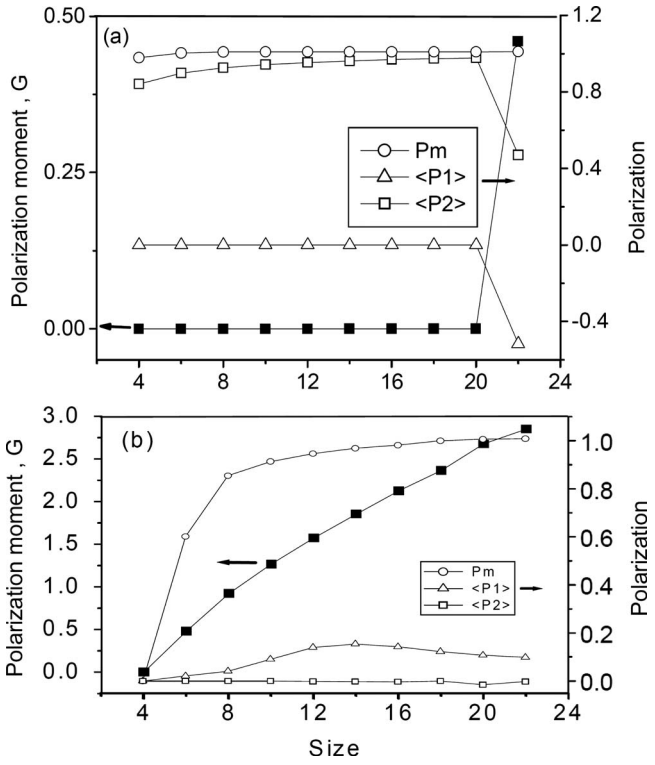

FIG. 6. The polarization moment G on the left vertical axis, and the macroscopically averaged polarization components, $\langle P_1\rangle$ and $\langle P_2\rangle$, and the magnitude of the maximum polarization P_m on the right vertical axis as functions of the sizes of the simulated ferroelectrics with $\beta=0$ in (a) and $\beta=1$ in (b) when a half level of LR-elastic interactions is taken into account ($\alpha=0.5$).

case of $\alpha=0$ and a nonzero value of the macroscopically averaged polarization $\langle P_1\rangle$ is produced. These differences are induced by LR-elastic interactions.

D. Influence of domain wall energy on the vortex structures

The values of gradient coefficients G_{ij} represent the strength of the gradient polarization energy density and may also play an important role in the formation of polarization patterns. To investigate the influence of gradient coefficients on the polarization pattern, a parameter γ is assigned to the gradient coefficients. When γ varies from 0 to 1, the gradient coefficients γG_{ij} change from 0 to G_{ij}. In the present work, we take the stress-free ferroelectrics under the open-circuit boundary condition ($\alpha=0$ and $\beta=1$) as a typical example to illustrate the effect of gradient coefficients. Figures 7(a)–7(d) show the polarization patterns in stress-free ferroelectrics with the size of 22 under the open-circuit condition by using different values of gradient coefficients γG_{ij} indicating that the number of domains decreases with the increase in gradient coefficient values. When the gradient coefficients are smaller, the gradient energy density is lower and it allows more domains to exists, as shown in Figs. 7(a) and 7(b). As γ increases to 0.6, the nanoparticle has a single-vortex structure, which is shown in Fig. 7(c), but the vortex center is not located at the simulated particle center. When γ further increases, the vortex center moves to the simulated particle center, as shown in Fig. 7(d). The vortex structure in Fig.

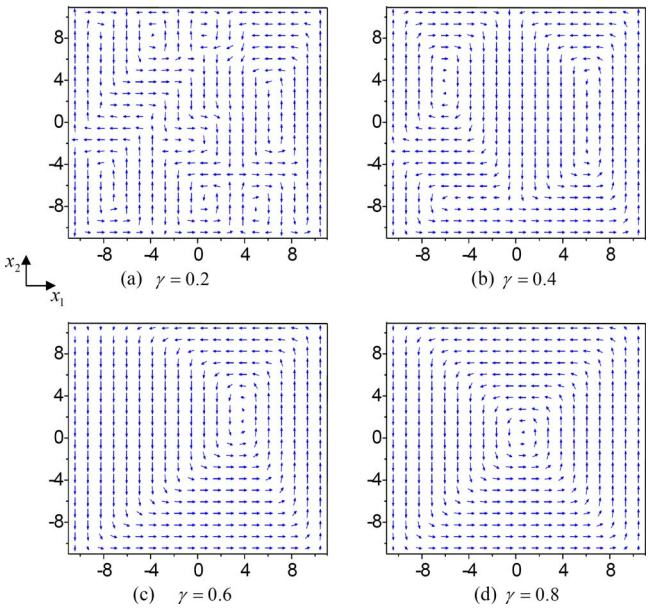

FIG. 7. (Color online) Polarization patterns in stress-free ferroelectric nanoparticles with different gradient coefficients γG_{ij} under the open-circuit condition. All nanoparticles have the same dimensionless size of 22.

7(d) will further change to that shown in Fig. 1(b) as γ equals 1. Figure 8 shows the polarization moment G on the left vertical axis, and the macroscopically averaged polarization components, $\langle P_1 \rangle$ and $\langle P_2 \rangle$, and the magnitude of the maximum polarization P_m on the right vertical axis, as functions of γ in the stress-free ferroelectrics under the open-circuit condition when the size of nanoparticles is 22. The polarization moment increases with increasing γ. When γ increases from 0.5 to 0.6, there is a jump in the polarization moment, which corresponds to the simulated ferroelectrics change from a multivortex structure to a single-vortex structure. The domain wall energy density is determined by the gradient coefficients. The larger the gradient coefficients are, the higher the domain wall energy density, and the less the total domain wall area will be. The simulation results verify this physical intuition and show that there is a transition from a multivortex structure to a single-vortex structure when the domain wall energy density increases.

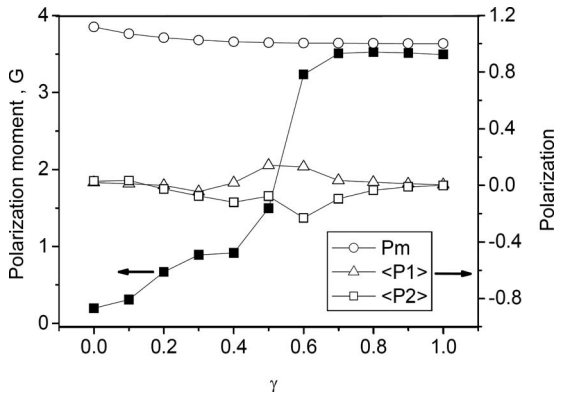

FIG. 8. The polarization moment G on the left vertical axis, and the macroscopically averaged polarization components, $\langle P_1 \rangle$ and $\langle P_2 \rangle$, and the magnitude of the maximum polarization P_m on the right vertical axis as functions of the γ in the stress-free ferroelectric nanoparticles under the open-circuit condition. All nanoparticles have the same dimensionless size of 22.

IV. CONCLUSIONS

In summary, the 2D phase field simulations demonstrate that LR-electrostatic and -elastic interactions and the particle size play a significant role in the formation of polarization patterns in ferroelectric nanoparticles. For a stress-free ferroelectric nanoparticle without any LR-elastic interactions, a vortex pattern with a purely toroidal moment of polarizations and macroscopically negligible averaged polarizations is formed if LR-electrostatic interactions are fully taken into account. This observed behavior is independent of the nanoparticle size ranging from 4 to 22. However, there is no vortex pattern in the ferroelectric nanoparticles if LR-electrostatic interactions are completely screened. When there are spontaneous strains associated with spontaneous polarizations, an internal stress field is usually induced in a freestanding ferroelectric nanoparticle even under the traction-free boundary condition. In this case, a monodomain structure or a multidomain structure can be formed, which is determined by the competition between LR-elastic and -electrostatic interactions. Since the strength of a depolarization field depends on the electric boundary condition, the electric boundary condition will play an important role in the formation of polarization patterns. To reduce the depolarization field energy, multidomain structures with 180° domain walls are energetically favorable, while monodomain structures and multidomain structures with 90° domain walls are energetically favorable to reduce the elastic energy. Ferroelectric nanoparticles with different levels of LR-elastic interactions may form a similar monodomain structure under the short-circuit boundary condition when the particle size is small. In addition, the vortex structure is dependent on the values of polarization gradient coefficients or the domain wall energy density. There exists a transition from a multivortex structure to a single-vortex structure when the domain wall energy density increases. The simulation results provide instructive information about the condition, under which the switchable toroidal moment of polarizations is stable. The switchable toroidal moment of polarizations may be used for future ultrahigh density data storing because it can be switched from one stable vortex state to the other by using a time-dependent magnetic field.

ACKNOWLEDGMENTS

J.W. gratefully acknowledges the Alexander von Humboldt Foundation for awarding a research fellowship to support his stay at Forschungszentrum Karlsruhe. T.Y.Z. is grateful for the support of the Hong Kong Research Grants Council under Grant No. G_HK015/06-II and the support from HKUST under Grant No. DAG05/06.EG35.

[1] K. Lee, K. Kim, S. J. Kwon, and S. Baik, Appl. Phys. Lett. **85**, 4711 (2004).
[2] M. W. Chu, I. Szafraniak, R. Scholz, C. Harnagea, D. Hesse, M. Alexe, and U. Gosele, Nature Mater. **3**, 87 (2004).
[3] V. Nagarajan, S. Prasertchoung, T. Zhao, H. Zheng, J. Ouyang, R. Rameshb, W. Tian, X. Q. Pan, D. M. Kim, C. B. Eom, H. Kohlstedt, and R. Waser, Appl. Phys. Lett. **84**, 5225 (2004).
[4] A. Roelofs, T. Schneller, K. Szot, and R. Waser, Appl. Phys. Lett. **81**, 5231 (2002).
[5] J. Junquera and P. Ghosez, Nature (London) **422**, 506 (2003).

[6]T. M. Shaw, S. Trolier-McKinstry, and P. C. McIntyre, Annu. Rev. Mater. Sci. **30**, 263 (2000).
[7]D. D. Fong, G. B. Stephenson, S. K. Streiffer, J. A. Eastman, O. Auciello, P. H. Fuoss, and C. Thompson, Science **304**, 1650 (2004).
[8]C. H. Ahn, K. M. Rabe, and J.-M. Triscone, Science **303**, 488 (2004).
[9]Y. Luo, I. Szafraniak, V. Nagarajan, R. B. Wehrspohn, M. Steinhart, J. H. Wendorff, N. D. Zakharov, R. Ramesh, and M. Alexe, Integr. Ferroelectr. **59**, 1513 (2003).
[10]G. Suyal, E. Colla, R. Gysel, M. Cantoni, and N. Setter, Nano Lett. **4**, 1339 (2004).
[11]B. Jiang, J. L. Peng, L. A. Bursill, and W. L. Zhong, J. Appl. Phys. **87**, 3462 (2000).
[12]W. L. Zhong, Y. G. Wang, P. L. Zhang, and B. D. Qu, Phys. Rev. B **50**, 698 (1994).
[13]W. S. Yun, J. J. Urban, Q. Gu, and H. Park, Nano Lett. **2**, 447 (2002).
[14]J. Wang and T. Y. Zhang, Phys. Rev. B **73**, 144107 (2006).
[15]J. Wang, S. Q. Shi, L. Q. Chen, Y. L. Li, and T. Y. Zhang, Acta Mater. **52**, 749 (2004).
[16]Y. L. Li, S. Y. Hu, Z. K. Liu, and L. Q. Chen, Acta Mater. **50**, 395 (2002).
[17]I. Ponomareva, I. I. Naumov, and L. Bellaiche, Phys. Rev. B **72**, 214118 (2005).
[18]S. Nambu and D. A. Sagala, Phys. Rev. B **50**, 5838 (1994).
[19]H. L. Hu and L. Q. Chen, Mater. Sci. Eng., A **238**, 182 (1997).
[20]R. Ahluwalia and W. Cao, J. Appl. Phys. **93**, 537 (2003).
[21]W. Cao, S. Tavener, and S. Xie, J. Appl. Phys. **86**, 5739 (1999).
[22]Y. L. Li, S. Y. Hu, Z. K. Liu, and L. Q. Chen, Appl. Phys. Lett. **81**, 427 (2002).
[23]J. Wang and T. Y. Zhang, Appl. Phys. Lett. **88**, 182904 (2006).
[24]M. E. Lines and A. M. Glass, *Principles and Applications of Ferroelectrics and Related Materials* (Clarendon, Oxford, 1977).
[25]I. I. Naumov, L. Bellaiche, and H. Fu, Nature (London) **432**, 737 (2004).